Nuclear Materials and Energy 46 (2026) 102091

Contents lists available at ScienceDirect

Nuclear Materials and Energy

journal homepage: www.elsevier.com/locate/nme

Deuterated ammonia formation, transport and dissociation in Ohmically-heated and nitrogen-seeded JET plasmas with low-recycling conditions at the divertor targets☆

R. Mäenpää [a,*], M. Groth [a], H. Kumpulainen [a], A.G. Meigs [b], E. Pawelec [c], D. Reiter [d], J. Romazanov [e], S. Brezinsek [e], A. Shaw [b], JET Contributors [1], EUROfusion Tokamak Exploitation Team [2]

[a] Aalto University, Espoo, Finland
[b] UKAEA, Abingdon, United Kingdom
[c] University of Opole, Institute of Physics, Opole, Poland
[d] Institute for Laser and Plasma Physics, Heinrich-Heine-University, Düsseldorf, Germany
[e] Forschungszentrum Jülich GmbH, Jülich, Germany

ARTICLE INFO

Keywords:
Nitrogen
Ammonia
Molecule
Recycling
JET
Divertor
EDGE2D-EIRENE
ERO2.0
AMMONX

ABSTRACT

A new deuterated ammonia (ND_3) formation, transport and dissociation model implemented in the ERO2.0 Monte Carlo-code predicts a peak line-integrated deuterated imidogen radical (ND) band emission intensity 50% higher than measured by the vertically-viewing divertor spectrometer in low-recycling, Ohmically-heated and nitrogen-seeded Joint European Torus (JET) plasmas. By assuming a greater kinetic energy release (KER) of 10 eV instead of 1 eV upon the dissociation of ND_3 and its radicals, the model predicts a peak line-integrated ND band emission intensity 25% lower than measured. Together these predictions support the assumption of thermal re-release of incident nitrogen atoms and ions from the divertor targets as nitrogen molecules (N_2) and ND_3 in equal fractions.

Band emission from the ND radical has previously been measured in nitrogen-seeded divertor plasmas in the JET and ASDEX Upgrade tokamaks. The proposed model makes use of the AMMONX database for electron-impact dissociation and ionization rates of ND_3 molecules and its dissociation products, and recent computational estimates of the electron-impact excitation rates of the ND radical. The assumption of thermal re-release of incident nitrogen ions and atoms as N_2 and ND_3 in equal fractions is also consistent with the maximum rates of ammonia production observed in measurements of tokamak divertor plasmas as well as with measurements performed in laboratory plasma devices with high surface fluxes of reactive hydrogen and nitrogen species.

1. Introduction

Nitrogen gas injection has been used to mitigate divertor heat loads and improve confinement in tokamaks with metallic plasma-facing components such as ASDEX Upgrade [1] and JET [2], but carries with it the potential for tritiated ammonia (NT_3, NDT_2 or ND_2T) formation in the deuterium–tritium plasma of a reactor [3]. As a polar molecule, (tritiated) ammonia desorption from cryopump surfaces occurs at higher temperatures than e.g. hydrogenic molecules and thus tritiated ammonia formation could impact the duty cycle of a reactor by necessitating more frequent high-temperature regenerations to avoid exceeding the cryopump tritium inventory limits [3]. In [4], an ammonia transport and dissociation model was implemented using the SOLPS-ITER code [5] and used to predict ammonia densities in an ITER deuterium, helium and nitrogen plasma. The predicted ammonia densities were found to be sensitive to the surface chemistry, which was simplified by imposing a fraction of nitrogen (N_2) molecules incident on solid surfaces to be re-released as ammonia or its radicals.

☆ This article is part of a Special issue entitled: 'PFMC-20' published in Nuclear Materials and Energy.

* Correspondence to: Aalto University, Otakaari 1, 02150 Espoo, Finland
E-mail address: roni.maenpaa@aalto.fi (R. Mäenpää).

[1] See the author list of "Overview of T and D-T results in JET with ITER-like wall" by C. F. Maggi et al. Nuclear Fusion **64** 112012 10.1088/1741-4326/ad3e16

[2] See the author list of "Overview of the EUROfusion Tokamak Exploitation programme in support of ITER and DEMO" by E. Joffrin et al. Nuclear Fusion **64** 112019 10.1088/1741-4326/ad2be4

https://doi.org/10.1016/j.nme.2026.102091
Received 14 July 2025; Received in revised form 21 February 2026; Accepted 25 February 2026
Available online 26 February 2026

Validating a model of ammonia formation, transport and dissociation against experiment would be a step towards (1) identifying techniques for minimizing the formation of ammonia and (2) predicting the need for high-temperature regenerations of the cryopump in a potential future reactor operating with nitrogen seeding. In this contribution, we model the formation, transport and dissociation of deuterated ammonia (ND_3) in low-recycling, Ohmically-heated and nitrogen-seeded plasmas in JET using the electron-impact dissociation and ionization rates from [4] and compare the predicted, line-integrated band emission from the deuterated imidogen radical (ND) to measurements. The surface chemistry is simplified by assuming that ND_3 is formed by nitrogen atoms and ions (not N_2 molecules) incident on divertor targets and main chamber walls reacting with deuterium incident from the plasma phase or already present at the surface. The formation rate of ND_3 is based on experimental data from laboratory plasma devices [6] and tokamak divertors [7]. The model is implemented in the ERO2.0 code [8], originally chosen for its capability to account for complex, three-dimensional plasma-facing structures. These capabilities are, however, not leveraged in this work.

2. Divertor spectroscopy of nitrogen ions and ND radicals in an Ohmic JET low-recycling plasma

Measurements by vertically-viewing fibre-optic [9] and mirror-link [10] divertor spectrometer systems (JET diagnostics KS3O/KSRA and KT3A, respectively) in a low-recycling, Ohmically-heated and nitrogen-seeded plasma in JET [11] (JET pulse number 81429, $t = 60$ s) are used in this work. Because the ammonia molecule itself does not have strong emission bands in the visible part of the electromagnetic spectrum, the mirror-link divertor spectrometer was set to observe the spectral region around 336 nm, where the ND radical, a dissociation product of ND_3, has its strongest emission band. The ND emission band around 336 nm due to the $A^3\Pi \rightarrow X^3\Sigma^-$ electronic transition is fitted using the procedure described in [12] (see Fig. B.7 for example spectra and fits). Line emission at 500 nm from N II (spectroscopic notation for N^+) was measured by the survey spectrometer (KSRA) of the fibre-optic divertor spectroscopy system (KS3O).

During the pulse, nitrogen gas (N_2) was injected into the low-field side (LFS) scrape-off layer (SOL) from a gas injection module (GIM9) toroidally distributed across 24 locations at a rate of approximately 4.9×10^{20} nitrogen atom equivalents per second. The low-field side strikepoint was located on the nearly-horizontal bulk tungsten target (JET tile 5, Fig. 1). The toroidal magnetic field was 2.2 T, the plasma current 2.0 MA and the line-integrated edge density measured by far-infrared interferometry [13] (JET diagnostic KG1V/LID4) was approximately 1.2×10^{19} m^{-3} at $t = 60$ s. The Ohmic heating power was approximately 1.3 MW during the flat-top phase of the pulse. Ionizing plasma conditions were measured by Langmuir probes near the low-field side strike point (electron temperature T_e = 20 eV to 25 eV, electron density $n_e = 0.6\times10^{19}$ m^{-3} to 1.0×10^{19} m^{-3}, Fig. 2). The temperature at the strike point was approximately 375 °C at $t = 60$ s, measured by a divertor-viewing infrared camera (JET diagnostic KL9B) [14]. Pulse 81429 was preceded by eight nitrogen-seeded pulses with varying densities and N_2 injection rates (nitrogen saturation has been shown to be a necessary condition for ammonia production on tungsten surfaces in laboratory plasma devices [15] - in an ASDEX Upgrade experiment, three consequent nitrogen-seeded discharges were sufficient to achieve saturation [16]).

3. Setup of EDGE2D-EIRENE simulations

EDGE2D-EIRENE [17,18] simulations (Table A.2) are used in this work to create a background plasma solution (of electron density n_e, electron temperature T_e, ion temperature T_i, parallel electric field $E_\parallel$ and parallel flow velocity $v_\parallel$) for ERO2.0. A grid based on the magnetic geometry of JET pulse number (JPN) 80295 [19] is used in the EDGE2D-EIRENE simulations of this work, as a grid based on JPN 81429 was not readily available. In JPN 80295, the toroidal field was 2.0 T and the plasma current 2.0 MA, and thus the connection length was approximately 9% smaller than in JPN 81429. The X-point and strike-point locations in JPN 80295 were approximately the same as those in JPN 81429 (Fig. 1).

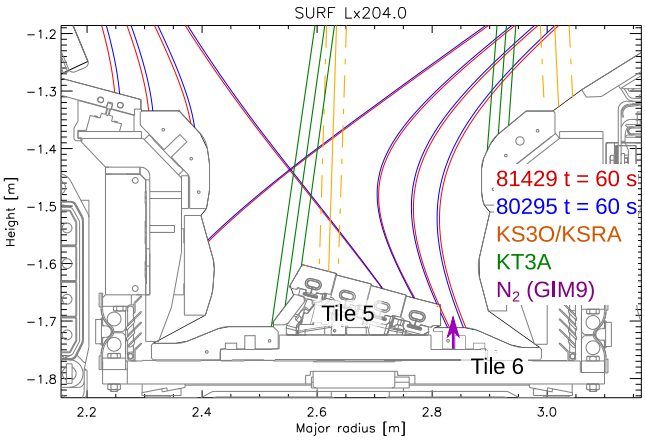

Fig. 1. Divertor geometry and magnetic configuration of JPN 81429 and 80295 at $t = 60$ s based on the pressure-constrained EFIT [20] equilibrium reconstruction. The scrape-off layer flux surfaces are separated by 1 cm at the low-field side midplane. The three radially innermost and outermost lines of sight of the KT3A system, and the radially innermost and outermost lines of sight of the KS3O/KSRA system (including their widths indicated by dashed lines) are shown. The poloidal location of the toroidally distributed gas injection module (GIM9) is marked with an arrow.

In the simulations, the electron density at the low-field side midplane separatrix ($n_{e,\ sep,\ LFS\text{-}mp}$) is adjusted using feedback injection of D_2 from the top of the plasma to match the EDGE2D-EIRENE-predicted plasma conditions to Langmuir probe measurements (JET diagnostic KY4D) at the low-field side divertor target (Fig. 2). When $n_{e,\ sep,\ LFS\text{-}mp}$ is set to 7.5×10^{18} m^{-3}, the predicted peak values of n_e and T_e are within approximately 20% of the measured peak values, but the predicted n_e and T_e peaks are distanced from the measured peaks by approximately 1 cm towards the LFS and HFS, respectively. Simultaneously matching the EDGE2D-EIRENE-predicted peak locations of n_e and T_e to less than 1 cm of the measured peak locations has proven difficult [21]). The predicted n_e and T_e are within approximately 20% of the measured values in the far scrape-off layer ($3\text{ cm} < R - R_{sep} < 11\text{ cm}$) when $n_{e,\ sep,\ LFS\text{-}mp}$ is set to 7.5×10^{18} m^{-3}. All EDGE2D-EIRENE simulations in this work include drifts, non-ambipolar electric fields and currents. The divertor targets and main chamber walls are assumed to consist of pure tungsten and beryllium, respectively. Sputtering and transport of beryllium are taken into account in the simulations, whereas tungsten sputtering and nitrogen injection are not included.

The power entering the EDGE2D-EIRENE computational domain across the core boundary (at $\rho_N = 0.8$) is set to 1.0 MW (assuming that 300 kW is radiated from inside the core boundary) and distributed equally between the electron and ion channels. The electron and ion heat diffusivities are set to spatially constant values of 1.0 m^2 s^{-1}. The main ion diffusivity is set to 1.0 m^2 s^{-1} in the private flux region, to 0.25 m^2 s^{-1} in an area around the separatrix extending 1 cm radially in either direction (the transport barrier), to 0.5 m^2 s^{-1} radially inward of the transport barrier and to 1.5 m^2 s^{-1} radially outward of the transport barrier. The diffusivity of beryllium ions is set to 1.0 m^2 s^{-1} throughout the computational domain. The pinch velocities of all ions are set to zero.

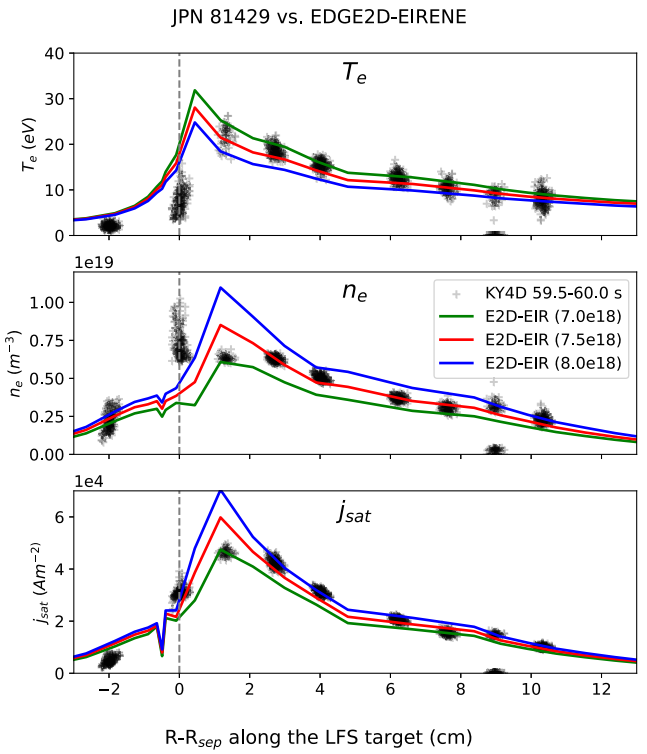

Fig. 2. Langmuir probe measurements of ion saturation current and inferred electron temperatures and electron densities from JPN 81429 at t = 59.5 s to 60.0 s (grey markers) versus EDGE2D-EIRENE predictions using different values of low-field side midplane separatrix electron density $n_{e,\,sep,\,LFS\text{-}mp}$ (solid lines, value of $n_{e,\,sep,\,LFS\text{-}mp}$ inside parentheses in units of m^{-3}). To account for the uncertainty of the separatrix location in the EFIT equilibrium reconstruction, the Langmuir probe data have been shifted towards the low-field side by 1.4 cm in R-space so that the maximum of electron density coincides with the strike point.

4. Setup of ERO2.0 simulations

The 3D Monte Carlo trace-impurity code ERO2.0 [8] is used in this work to model N_2 injection, transport and dissociation, leading to ND_3 formation, transport and dissociation. The ERO2.0 simulations in this work (Table A.2) use an axisymmetric model of the JET plasma-facing components and an axisymmetric background plasma solution from EDGE2D-EIRENE (with $n_{e,\,sep,\,LFS\text{-}mp}$ set to 7.5×10^{18} m^{-3}, see Section 7 for a discussion on sensitivity). The EDGE2D-EIRENE background plasma solution contains axisymmetric distributions of the electron and main ion (D^+) densities, the electron and ion temperatures, the main ion parallel flow velocity and the parallel electric field. The diffusivity of all nitrogens ions is set to 1.0 $m^2\,s^{-1}$ as in [22], and the pinch velocity to zero. The ERO2.0 transport calculation is linear (impurity molecules, atoms and ions do not interact with each other) and the background plasma remains static.

In the ERO2.0 simulations, nitrogen is injected axisymmetrically as N_2 molecules (although injection as N_2 molecules has an insignificant effect on predicted nitrogen ion densities when compared to injection as atoms as shown in [22]) into the low-field side scrape-off layer at the poloidal location of gas injection module 9 (GIM9, Fig. 1). The N_2 injection rate is treated in the ERO2.0 simulations as a free parameter, and is adjusted to approximately match the predicted line-integrated N II peak intensity to the measurements by the vertically-viewing fibre-optic divertor spectrometer (KS3O/KSRA). Electron-impact ionization rates of nitrogen atoms and ions are taken from the OPEN-ADAS database [23] (these data were identical to the ionization rates available from the ADAS package on the JET Data Center cluster at the time of this study).

Table 1
Reaction identifiers from AMJUEL (2.7.5 to 2.7.12) and AMMONX (07 to ZC), reaction equations and kinetic energy release (KER) values for the electron-impact reactions of N_2, NH_3, NH_2, NH and their singly-charged molecular ions included in the ERO2.0 simulations. KER values separated by forward slashes indicate different values used in the sensitivity analysis. The impacting electron has been subtracted from the reaction equations for brevity (except in the case of the dissociative recombination reactions 24, 25 and 28).

Ident.	Reaction	KER (eV)
2.7.5	$N_2 \longrightarrow 2N$	0.95
2.7.9	$N_2 \longrightarrow e + N_2^+$	0.0
2.7.10	$N_2 \longrightarrow e + N + N^+$	8.0
2.7.11	$N_2^+ \longrightarrow e + 2N^+$	11.8
2.7.12	$N_2^+ \longrightarrow N + N^+$	1.0
07	$NH \longrightarrow NH^+ + e$	0.0
08	$NH \longrightarrow N^+ + H + e$	0.1/1.0/10.0
09	$NH_2 \longrightarrow NH_2^+ + e$	0.0
10	$NH_2 \longrightarrow NH^+ + H + e$	0.1/1.0/10.0
11	$NH_3 \longrightarrow NH_3^+ + e$	0.0
12	$NH_3 \longrightarrow NH_2^+ + H + e$	0.1/1.0/10.0
15	$NH \longrightarrow N + H$	0.1/1.0/10.0
16	$NH_2 \longrightarrow N + H_2$	0.1/1.0/10.0
17	$NH_2 \longrightarrow NH + H$	0.1/1.0/10.0
18	$NH_3 \longrightarrow NH_2 + H$	0.1/1.0/10.0
19	$NH_3 \longrightarrow NH + H_2$	0.1/1.0/10.0
24	$e + NH^+ \longrightarrow N + H$	0.1/1.0/10.0
25	$e + NH_2^+ \longrightarrow NH + H$	0.1/1.0/10.0
28	$e + NH_3^+ \longrightarrow NH_2 + H$	0.1/1.0/10.0
ZC	$NH_3 \longrightarrow H^+ + NH_2 + e$	0.1/1.0/10.0

Nitrogen ions and atoms incident on the divertor targets or main chamber walls in the ERO2.0 simulations either undergo fast reflection, or are re-released as either N_2 or ND_3 with a thermal energy corresponding to the temperature of the plasma-facing component (i.e., recycled). The particle and energy reflection coefficients have been calculated using the SDTrimSP-code [24]. In this work, we have assumed a spatially uniform plasma-facing component temperature of 300 °C (cf. the strike point temperature 375 °C at t = 60 s), i.e. the energy of the recycled (monoenergetic) molecules is $\frac{3}{2}k_B T_{wall} = 0.074$ eV. Nitrogen ions and atoms incident on plasma-facing components that do not undergo fast reflection are assumed to recycle as either N_2 or ND_3 in equal fractions (see Section 7 for discussion). A pump with a species-independent albedo of 0.94 is included in the low-field side divertor corner as in [25] (see Section 7 for a discussion on the sensitivity of the predictions on the assumed pump albedo).

Five electron-impact dissociation and ionization reactions [26] for N_2 and singly-charged molecular ions (N_2^+) are included in ERO2.0 (Table 1). In this work, the kinetic energy release (KER) values, i.e. the total translational energy imparted onto the dissociation fragments, are taken from the AMJUEL database [27] for the N_2 and N_2^+ reactions. Additionally, 15 electron-impact dissociation and ionization reactions for ammonia, its radicals and their singly-charged molecular ions from the AMMONX database [4] are included (see Section 7 for discussion). The AMMONX database does not contain KER values, and thus a sensitivity study is conducted by using 0.1, 1.0 or 10.0 eV as the kinetic energy release value for the dissociative reactions (cf. [28], where KER values of 1.8 eV to 10.6 eV were measured for the electron-impact dissociation of NH_3).

Photon emissivity coefficients from the OPEN-ADAS database (identical to the photon emissivity coefficients available from the ADAS package at the JET Data Center cluster) are used to relate the ERO2.0-predicted N^+ density to the photon emission rates (in ph $m^{-3}\,sr^{-1}\,s^{-1}$) of

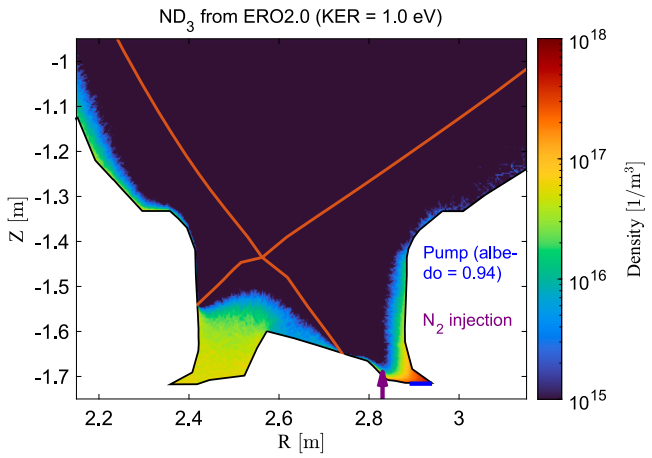

Fig. 3. Density of ND_3 predicted by ERO2.0, assuming that 1.0 eV of translational energy is imparted onto the dissociation fragments in reactions 07 to ZC in Table 1. An average over the toroidal direction and over four time steps is shown. The separatrix (solid red line) corresponds to the magnetic geometry used in the EDGE2D-EIRENE simulations. The locations of the N_2 injection and the pump surface are marked with a purple arrow and blue line, respectively.

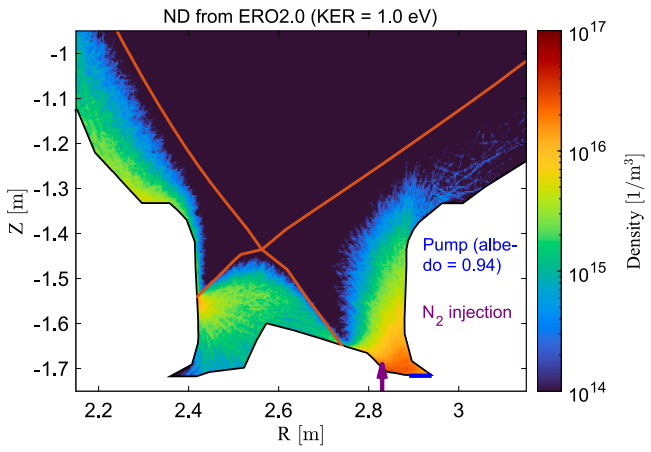

Fig. 4. Density of ND predicted by ERO2.0, assuming that 1.0 eV of translational energy is imparted onto the dissociation fragments in reactions 07 to ZC in Table 1. An average over the toroidal direction and over four time steps is shown. The separatrix (solid red line) corresponds to the magnetic geometry used in the EDGE2D-EIRENE simulations. The locations of the N_2 injection and the pump surface are marked with a purple arrow and blue line, respectively.

the 500 nm N II line. To relate the predicted density of the ND radical to the 336 nm band emission rate, we assume that the excitation of the ND radical occurs due to electron-impact only, that the electronically excited ND state ($A^3\Pi$) decays instantaneously via photon emission to the electronic ground state ($X^3\Sigma^-$), and that no absorption of the emitted photon takes place in the plasma (i.e. we assume coronal conditions). A theoretical estimate of the $X^3\Sigma^- \rightarrow A^3\Pi$ electron-impact excitation cross-section from [29] is convolved with a Maxwellian electron energy distribution function to obtain a rate coefficient. The predicted photon emission rates of the N II 500 nm line and the ND 336 nm band are integrated along the lines of sight of the vertically-viewing divertor spectroscopy systems (KS3O/KSRA and KT3A, respectively).

5. Spatial distribution of deuterated ammonia and its dissociation products in the divertor

ERO2.0 predicts that ND_3 is concentrated in the low-field side divertor corner (Fig. 3), irrespective of the assumed kinetic energy release value of the dissociation reactions of ammonia and its radicals (reactions 07 to ZC in Table 1). The predicted density of ND_3 in the high-field side divertor corner is increased severalfold if a kinetic energy release value of 10.0 eV instead of 0.1 eV is assumed for reactions 07 to ZC. Irrespective of the assumed kinetic energy release value, predicted ND_3 densities are higher above the high-field side divertor entrance than above the low-field side divertor entrance due to the vertical target configuration and the subsequently higher nitrogen ion flux directed at the first wall above the high-field divertor entrance.

ERO2.0 predicts that the (neutral) dissociation products of ND_3, i.e. ND_2 (figure omitted) and ND (Fig. 4), are concentrated in the low-field side divertor, and that ND_2 and ND are also present in the high-field side corner and above the high-field side divertor entrance. The predicted density of ND_2 in the low-field side divertor corner is approximately twice as high as the density of ND. Assuming a kinetic energy release value of 10.0 eV for reactions 07 to ZC leads ERO2.0 to predict ND and ND_2 densities approximately an order of magnitude lower in the low-field side divertor corner compared to when 0.1 eV is assumed. The decrease in predicted density associated with higher kinetic energy release values is due to the higher velocities and correspondingly shorter lifetimes of the dissociation fragments before ionization or further dissociation. Higher assumed kinetic energy release values also increase the penetration of the dissociation fragments into the plasma.

6. Line-integrated emission from N II and ND

The peak N II 500 nm line-integrated intensity predicted by ERO2.0 is within the uncertainty of the peak intensity measured by the fibre-optic divertor spectroscopy system (Fig. 5) when N_2 is injected (and pumped) at a rate of 1×10^{19} N atom equivalents per second, assuming that either 0.1 eV or 1.0 eV of kinetic energy is imparted onto the dissociation fragments in reactions 07 to ZC of Table 1. Assuming that 10.0 eV is imparted onto the dissociation fragments instead, the predicted N II 500 nm peak intensity is approximately 20% higher than the measured intensity when the same injection rate is used. In all three cases, the predicted profiles of line-integrated intensity are narrower than the measured profile, and the predicted peaks are distanced from the measured peak by approximately 5 cm towards the low-field side (see Section 7 for discussion). The N_2 injection rate in the simulations (1×10^{19} N atom equivalents per second) is lower than in the experiment (4.9×10^{20} N atom equivalents per second) by approximately a factor of 50, possibly due to an overestimation of the pump albedo or the lack of physics models describing the increase in transport of the injected N_2 from the injection site into the pump in the low-field side divertor corner (see also Section 7 for discussion).

The peak line-integrated intensity of the ND emission band around 336 nm predicted by ERO2.0 (Fig. 6), as well as the spatial distribution of the line-integrated intensity, is more sensitive to the assumed kinetic energy release value of reactions 07 to ZC than the N II 500 nm line-integrated intensity. By assuming a kinetic energy release of 1.0 eV, ERO2.0 predicts a peak line-integrated intensity 50% higher than measured in the low-field side scrape-off layer, whereas if 10.0 eV is assumed to be released, ERO2.0 predicts a peak line-integrated intensity 25% lower than measured in the low-field side scrape-off layer. The measured ND peak emission in the low-field side scrape-off layer is thus bracketed from above and below by the predicted peak ND emission (assuming a 1.0 eV or 10.0 eV kinetic energy release, respectively), which we interpret as tentative support for the present model of ammonia formation, transport and dissociation, including the hypothesis of nitrogen recycling as N_2 and ND_3 in equal fractions (with the caveat that the N_2 injection rate is treated as a free parameter in the ERO2.0 simulations).

When 10.0 eV of kinetic energy is assumed to be released in reactions 07 to ZC, the spatial distribution of the predicted line-integrated intensity is broader and more consistent with measurements than if 1.0 eV or

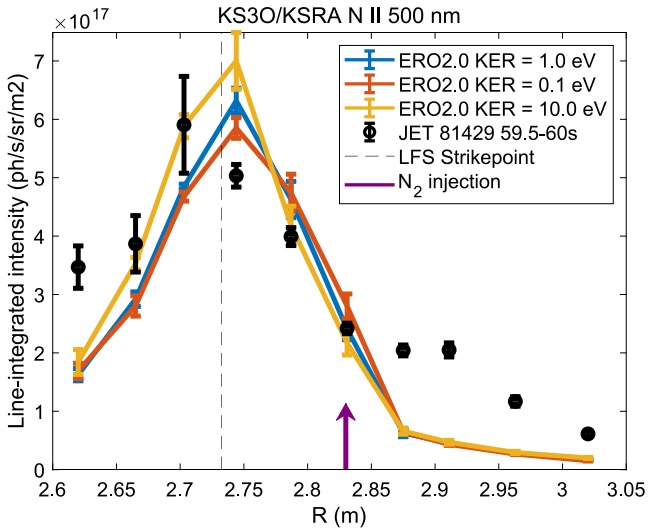

Fig. 5. Line-integrated intensity of the N II 500 nm transitions measured by the outer divertor fibre-optic spectroscopy system (KS3O) survey spectrometer (KSRA) in JET pulse number 81429 averaged over the interval t = 59.5 s to 60.0 s and the line-integrated intensities predicted by ERO2.0 assuming that either 0.1 eV, 1.0 eV or 10.0 eV of kinetic energy is imparted onto the dissociation fragments in reactions 07 to ZC in Table 1. Error bars represent standard deviations over the time interval (measurement) or standard deviations over iterations/time steps (ERO2.0 predictions). The radial locations of the low-field side strikepoint and the N_2 injection are marked with a dashed grey line and a purple arrow, respectively.

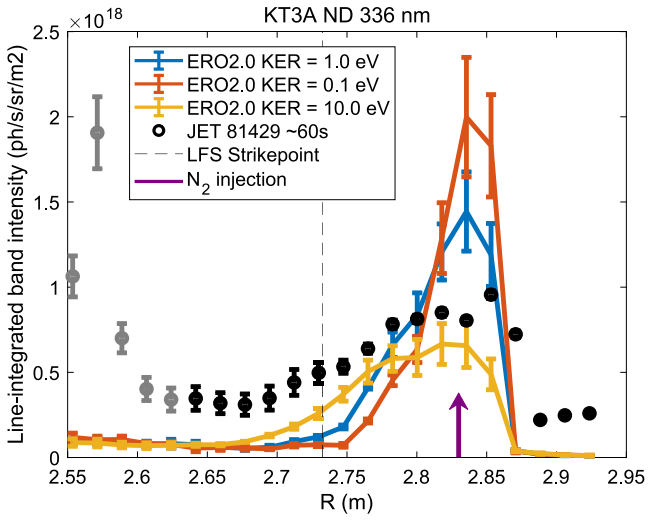

Fig. 6. Line-integrated intensity of ND band emission around 336 nm measured by the vertically-viewing mirror-link divertor spectrometer system (KT3A) in JET pulse number 81429 at $t \approx 60$ s, and line-integrated intensities predicted by ERO2.0, assuming that either 0.1 eV, 1.0 eV or 10.0 eV of kinetic energy is imparted onto the dissociation fragments in reactions 07 to ZC in Table 1. Error bars are derived from the fitting procedure (measurement) or represent standard deviations over iterations/time steps (ERO2.0 predictions). Data points likely affected by artefacts from the fitting procedure have been greyed out. The radial locations of the low-field side strikepoint and the N_2 injection are marked with a dashed grey line and a purple arrow, respectively.

0.1 eV is assumed to be released. Irrespective of the assumed kinetic energy release value, ERO2.0 underpredicts the line-integrated ND band intensity from the peak towards the low-field side. Consistently, above the low-field side divertor shoulder, where the four radially outermost lines of sight of the KT3A mirror-link divertor spectrometer terminate (Fig. 1), the predicted ND densities are orders of magnitude lower compared to densities in e.g. the low-field side divertor corner (Fig. 4). The underprediction of ND emission at $R > 2.85$ m is attributed to the axisymmetric, fully-enclosed 3D model of the divertor structure, which does not allow neutral N_2 or ND_3 to travel from the LFS divertor corner to the divertor shoulder through the toroidal tile gaps and divertor support structures. The apparent peak of the line-integrated ND band emission intensity in the experimental data towards the high-field side is considered an artefact arising from the fitting procedure.

7. Discussion

In this work, nitrogen ions and atoms incident on divertor targets or main chamber walls that do not undergo fast reflection are recycled as N_2 or ND_3 molecules in equal fractions, an assumption which is predicated on two experimental studies. First, van Helden et al. [6] found that up to 48% of nitrogen gas, first dissociated in a plasma arc and then allowed to expand onto stainless steel surfaces was converted into ammonia, when the ratio of incident hydrogen atoms to nitrogen atoms was large (Fig. 14 in [6]). In [6], the possibility of plasma-phase reactions contributing to ammonia formation was excluded due to the low gas pressure in the experiment. We posit that in a low-recycling, Ohmically-heated and nitrogen-seeded divertor plasma, low-gas-pressure conditions also prevail, and the ratio of hydrogenic ions and atoms to nitrogen ions and atoms incident on the divertor targets and main chamber walls is also large. Additionally, van Helden et al. found that the ammonia formation efficiency was independent of the whether the reaction took place on a stainless steel surface or a layer of silicon nitride due to the high flux of reactive nitrogen and hydrogen atoms creating a passivated surface on which the formation of ammonia took place, making their results potentially applicable to the modelling of ammonia formation on the tungsten divertor surfaces of JET.

Second, Reichbauer et al. [7] found that up to 50% of nitrogen released from the divertor target and main chamber walls in an unseeded ASDEX Upgrade discharge formed ammonia. In discharges in which N_2 was seeded, it was found that a significant fraction of seeded N_2 was not dissociated in the plasma and thus could not form ammonia, resulting in lower ratios of ammonia to N_2 molecules measured by the residual gas analysers. Reichbauer et al. did not propose a mechanism for the N_2 molecules to bypass the plasma and enter the pumping plena directly in the ASDEX Upgrade experiment. In a JET experiment, approximately one third of the injected, isotopically-labelled methane ($^{13}CH_4$) was observed to be directly pumped [30], possibly due to the gas injection ports (GIM 9) being located underneath the divertor tiles (tile 6, Fig. 1). In the simulations conducted in this work, the N_2 molecules are injected into the plasma above the divertor tiles and then travel in straight trajectories until they are ionized, dissociated or impact a wall, and thus due to geometric reasons it is improbable for the injected N_2 to bypass the plasma and be pumped directly.

The lack of a bypass mechanism in the ERO2.0 simulations and an overestimation of the albedo of the pump (set to 0.94) are possible reasons to the discrepancy between the injection rate in the simulations (1×10^{19} N atom equivalents per second) and in the experiment (approximately 4.9×10^{20} N atom equivalents per second). The results, however, are insensitive to the assumed albedo of the pump, provided that the N_2 injection rate is treated as a free parameter: by decreasing the pump albedo to 0.4, and increasing the N_2 injection rate to 4.5×10^{19} N atom equivalents per second, the peak N II 500 nm and ND 336 nm intensities predicted by ERO2.0 are within 20% of the predicted peak intensities when an albedo of 0.94 and injection rate of 1.0×10^{19} N atom equivalents per second are used. Assessing the sensitivity of the results to a potential geometric bypass mechanism would require a detailed CAD model of the divertor structure from the gas injection ports to the cryopump, which was not available at the time of this study.

If the assumed electron density at the low-field side midplane separatrix ($n_{e,sep,LFS\text{-}mp}$) in the EDGE2D-EIRENE simulations is increased from 7.5×10^{18} m^{-3} to 8.0×10^{18} m^{-3}, ERO2.0 predicts that the peak line-integrated N II and ND intensities are increased by approximately 30% and 20%, respectively, when an N_2 injection rate of 1.0×10^{19} N atom equivalents per second and a pump albedo of 0.94 are used. Similarly, decreasing the assumed $n_{e,sep,LFS\text{-}mp}$ from 7.5×10^{18} m^{-3} to 7.0×10^{18} m^{-3} reduces the peak line-integrated N II and ND intensities predicted by ERO2.0 by approximately 5% and 20%, respectively. The radial location of the N II emission peak predicted by ERO2.0 is insensitive to the assumed $n_{e,sep,LFS\text{-}mp}$ in the EDGE2D-EIRENE simulations (in contrast to earlier modelling of partially-detached, low-confinement mode JET plasmas [22]). The discrepancy between the measured and predicted radial location of the N II emission peak is attributed to the EDGE2D-EIRENE predicted electron density peaking approximately 3 cm towards the low-field side compared to the (unshifted) electron density measured by Langmuir probes.

A subset of 15 reactions (Table 1) from the AMMONX database is included in the simulations of this work (rate coefficients for 183 reactions are listed in the database). Any reaction fulfilling one or more of the following criteria is not included in the ERO2.0 simulations in this work: (1) a rate coefficient for the reaction is already included in the ERO2.0 simulation, (2) the reaction involves a metastable N_2 molecule as a reactant or a product, (3) the reaction is not due to an electron impact, (4) the reaction involves N_2H, N_2H^+ or NH_4^+, either as a reactant or a product, or (5) the reaction has three or more heavy (non-electron) products. The inclusion of metastable N_2 molecules was shown in [4] to have negligible impact on the predicted ND_3 density, and hence metastable N_2 molecules are omitted in this work. In [31], electron-impact reactions were found to be the dominant loss mechanism of ammonia in a zero-dimensional model of H_2-N_2 plasmas with $T_e \approx 3$ eV to 5 eV, and thus ion-neutral and neutral–neutral reactions are excluded in the ERO2.0 simulations of $T_e \approx 10$ eV to 25 eV plasmas studied in this work. Furthermore, including ion-neutral or neutral–neutral chemistry between nitrogen-containing species would make the ERO2.0 simulation non-linear and potentially much more computationally demanding. Reactions involving NH_4^+ are omitted, as NH_4^+ is formed only in plasma-phase reactions between heavy (non-electron) reactants. Due to the lack of spectroscopic measurements and estimates of surface formation rates, N_2H and its molecular ion N_2H^+ are not included in the simulations. Finally, ERO2.0 does not currently support molecular dissociation reactions with three or more heavy products, and hence such reactions are not included.

8. Conclusions

A deuterated ammonia (ND_3) formation, transport and dissociation model implemented in ERO2.0 and applied to low-recycling, Ohmically-heated and nitrogen-seeded plasmas in JET predicts that ND_3 is concentrated in the low-field side divertor corner, and to a lesser degree in the high-field side divertor corner and above the high-field side divertor shoulder. Nitrogen atoms and ions incident on divertor targets and main chamber walls that do not undergo fast reflection are recycled as ND_3 or nitrogen molecules (N_2) in equal fractions, an assumption based on experimental findings in laboratory plasma devices [6] and tokamak divertor plasmas with a significant wall inventory of nitrogen but no active N_2 seeding [7]. Only electron-impact reactions (with two or fewer non-electron products) from the AMMONX database are included in the model due to the ionizing character of the low-recycling divertor plasma.

The predicted densities of ND_2 and ND in the low-field side divertor are found to be sensitive to the assumed kinetic energy release associated with the dissociation reactions of ND_3, ND_2 and ND due to the higher velocities and shorter lifetimes of the dissociation fragments leading to lower predicted densities. Band emission from the ND radical is predicted using cross-section data from theoretical estimates [29] and assuming that electron-impact excitation and spontaneous emission are the only mechanisms of excitation and de-excitation, respectively. Assuming that 1.0 eV of translational energy is imparted onto the dissociation fragments, ERO2.0 predicts a peak line-integrated ND band emission intensity approximately 50% higher than measured in the low-field side divertor volume. Assuming 10.0 eV to be imparted instead, ERO2.0 predicts a peak intensity 25% lower than measured with the spatial distribution of line-integrated intensity being broader and more consistent with the measurements.

ND band emission spectra have been measured in JET [12] and ASDEX Upgrade [32] high-confinement mode plasmas. Comparing the ND_3 dissociation and ND band emission models against these measurements would allow testing the hypothesis of nitrogen recycling as N_2 and ND_3 in equal fractions with higher plasma-facing component surface temperatures (W surface temperatures above 830 K have been shown to reduce ammonia production in N_2-H_2 radio frequency plasmas due to thermal decomposition [33]). Direct comparison of the model against residual gas analysis measurements in discharges with active N_2 seeding (as opposed to a legacy nitrogen inventory only) would necessitate the resolution of the discrepancy in the steady-state injection and pumping rates between the simulation and the experiment, possibly by introducing an accurate three-dimensional description of the divertor structure from the gas injection ports to the cryopump.

CRediT authorship contribution statement

R. Mäenpää: Writing – review & editing, Writing – original draft, Software, Methodology, Investigation, Funding acquisition, Conceptualization. **M. Groth:** Writing – review & editing, Supervision, Resources, Project administration, Investigation, Funding acquisition, Conceptualization. **H. Kumpulainen:** Software, Methodology, Conceptualization. **A.G. Meigs:** Software, Methodology, Investigation, Data curation. **E. Pawelec:** Methodology, Investigation, Data curation. **D. Reiter:** Methodology, Investigation, Conceptualization. **J. Romazanov:** Software, Methodology. **S. Brezinsek:** Supervision, Resources, Project administration, Conceptualization. **A. Shaw:** Data curation.

Declaration of competing interest

The authors declare that they have no known competing financial interests or personal relationships that could have appeared to influence the work reported in this paper.

Acknowledgements

This work has been carried out within the framework of the EUROfusion Consortium, funded by the European Union via the Euratom Research and Training Programme (Grant Agreement No 101052200 — EUROfusion). Views and opinions expressed are however those of the author(s) only and do not necessarily reflect those of the European Union or the European Commission. Neither the European Union nor the European Commission can be held responsible for them. This work made use of the Triton cluster, part of the Science-IT project at Aalto University.

Appendix A. Catalogue of simulations

See Table A.2.

Appendix B. Example spectra and fits

See Fig. B.7.

Table A.2
The ERO2.0 simulations are stored on the Aalto Triton cluster under "/scratch/phys/fusion/ero/runs/rmaenpaa/jet/" and the EDGE2D-EIRENE simulations are stored on the JET Data Centre cluster under "/home/rmaenpaa/cmg/catalog/edge2d/jet/80295/".

Code	Directory	Description
ERO2.0	run212/seq01	KER = 1.0 eV (07 to ZC)
	run213/seq01	KER = 0.1 eV (07 to ZC)
	run214/seq01	KER = 10.0 eV (07 to ZC)
E2D-EIR	aug0823/seq#1	$n_{e,sep,LFS\text{-}mp} = 7.0 \times 10^{18}$ m^{-3}
	jul3124/seq#1	$n_{e,sep,LFS\text{-}mp} = 7.5 \times 10^{18}$ m^{-3}
	jul3124/seq#2	$n_{e,sep,LFS\text{-}mp} = 8.0 \times 10^{18}$ m^{-3}

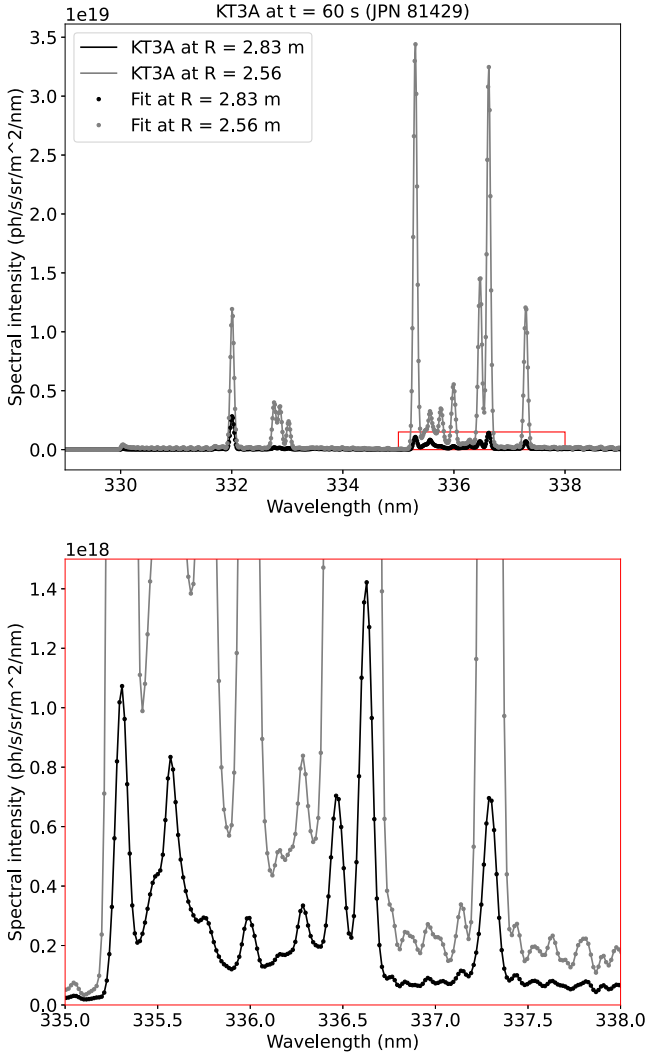

Fig. B.7. Spectral intensity at major radii $R = 2.56$ m and 2.83 m measured by the vertically-viewing mirror-link divertor spectrometer system (KT3A) in JET pulse number 81429 at $t \approx 60$ s, and the corresponding fits from the procedure described in [12]. The spectral region between 335 nm and 338 nm is shown on a different scale on the lower axes.

References

[1] A. Huber, M. Wischmeier, M. Bernert, S. Wiesen, S. Glöggler, S. Aleiferis, S. Brezinsek, G. Calabro, P. Carvalho, V. Huber, G. Sergienko, E.R. Solano, C. Giroud, M. Groth, S. Jachmich, C. Linsmeier, G.F. Matthews, A.G. Meigs, P. Mertens, M. Sertoli, S. Silburn, G. Telesca, JET contributors, Peculiarity of highly radiating multi-impurity seeded H -mode plasmas on JET with ITER-like wall, Phys. Scr. T171 (2020) 014055, http://dx.doi.org/10.1088/1402-4896/ab5753.

[2] M. Bernert, F. Janky, B. Sieglin, A. Kallenbach, B. Lipschultz, F. Reimold, M. Wischmeier, M. Cavedon, P. David, M. Dunne, M. Griener, O. Kudlacek, R. McDermott, W. Treutterer, E. Wolfrum, D. Brida, O. Février, S. Henderson, M. Komm, X-Point radiation, its control and an ELM suppressed radiating regime at the ASDEX upgrade tokamak, Nucl. Fusion 61 (2) (2021) 024001, http://dx.doi.org/10.1088/1741-4326/abc936.

[3] R. Pitts, X. Bonnin, F. Escourbiac, H. Frerichs, J. Gunn, T. Hirai, A. Kukushkin, E. Kaveeva, M. Miller, D. Moulton, V. Rozhansky, I. Senichenkov, E. Sytova, O. Schmitz, P. Stangeby, G. De Temmerman, I. Veselova, S. Wiesen, Physics basis for the first ITER tungsten divertor, Nucl. Mater. Energy 20 (2019) 100696, http://dx.doi.org/10.1016/j.nme.2019.100696.

[4] S. Touchard, J. Mougenot, C. Rond, K. Hassouni, X. Bonnin, AMMONX: A kinetic ammonia production scheme for EIRENE implementation, Nucl. Mater. Energy 18 (2019) 12–17, http://dx.doi.org/10.1016/j.nme.2018.11.020.

[5] S. Wiesen, D. Reiter, V. Kotov, M. Baelmans, W. Dekeyser, A. Kukushkin, S. Lisgo, R. Pitts, V. Rozhansky, G. Saibene, I. Veselova, S. Voskoboynikov, The new SOLPS-ITER code package, J. Nucl. Mater. 463 (2015) 480–484, http://dx.doi.org/10.1016/j.jnucmat.2014.10.012.

[6] J.H. Van Helden, W. Wagemans, G. Yagci, R.A.B. Zijlmans, D.C. Schram, R. Engeln, G. Lombardi, G.D. Stancu, J. Röpcke, Detailed study of the plasma-activated catalytic generation of ammonia in N2-H2 plasmas, J. Appl. Phys. 101 (4) (2007) 043305, http://dx.doi.org/10.1063/1.2645828.

[7] T. Reichbauer, A. Drenik, R. McDermott, V. Rohde, Assessment of nitrogen fluence from the divertor plasma in nitrogen seeded discharges, Fusion Eng. Des. 149 (2019) 111325, http://dx.doi.org/10.1016/j.fusengdes.2019.111325.

[8] J. Romazanov, D. Borodin, A. Kirschner, S. Brezinsek, S. Silburn, A. Huber, V. Huber, H. Bufferand, M. Firdaouss, D. Brömmel, B. Steinbusch, P. Gibbon, A. Lasa, I. Borodkina, A. Eksaeva, C. Linsmeier, JET Contributors, First ERO2.0 modeling of Be erosion and non-local transport in JET ITER-like wall, Phys. Scr. T170 (2017) 014018, http://dx.doi.org/10.1088/1402-4896/aa89ca.

[9] P.D. Morgan, K.H. Behringer, P.G. Carolan, M.J. Forrest, N.J. Peacock, M.F. Stamp, Spectroscopic measurements on the joint European torus using optical fibers to relay visible radiation, Rev. Sci. Instrum. 56 (5) (1985) 862–864, http://dx.doi.org/10.1063/1.1138074.

[10] A. Meigs, M. Stamp, R. Igreja, S. Sanders, P. Heesterman, JET-EFDA Contributors, Enhancement of JET's mirror-link near-ultraviolet to near-infrared divertor spectroscopy system, Rev. Sci. Instrum. 81 (10) (2010) 10E532, http://dx.doi.org/10.1063/1.3502322.

[11] M. Oberkofler, D. Douai, S. Brezinsek, J. Coenen, T. Dittmar, A. Drenik, S. Romanelli, E. Joffrin, K. McCormick, M. Brix, G. Calabro, M. Clever, C. Giroud, U. Kruezi, K. Lawson, C. Linsmeier, A. Martin Rojo, A. Meigs, S. Marsen, R. Neu, M. Reinelt, B. Sieglin, G. Sips, M. Stamp, F. Tabares, First nitrogen-seeding experiments in JET with the ITER-like wall, J. Nucl. Mater. 438 (2013) S258–S261, http://dx.doi.org/10.1016/j.jnucmat.2013.01.041.

[12] E. Pawelec, T. Dittmar, A. Drenik, A. Meigs, J. Contributors, Molecular ND band spectroscopy in the divertor region of nitrogen seeded JET discharges, J. Phys.: Conf. Ser. 959 (2018) 012009, http://dx.doi.org/10.1088/1742-6596/959/1/012009.

[13] A. Boboc, C. Gil, P. Pastor, P. Spuig, T. Edlington, S. Dorling, JET-EFDA Contributors, Upgrade of the JET far infrared interferometer diagnostic, Rev. Sci. Instrum. 83 (10) (2012) 10E341, http://dx.doi.org/10.1063/1.4737420.

[14] I. Balboa, G. Arnoux, T. Eich, B. Sieglin, S. Devaux, W. Zeidner, C. Morlock, U. Kruezi, G. Sergienko, D. Kinna, P.D. Thomas, M. Rack, JET EFDA Contributors, Upgrade of the infrared camera diagnostics for the JET ITER-like wall divertor, Rev. Sci. Instrum. 83 (10) (2012) 10D530, http://dx.doi.org/10.1063/1.4740523.

[15] F. Ghiorghiu, T. Aissou, M. Minissale, T. Angot, G. De Temmerman, R. Bisson, Nitrogen retention and ammonia production on tungsten, Nucl. Fusion 61 (12) (2021) 126067, http://dx.doi.org/10.1088/1741-4326/ac3698.

[16] M. Oberkofler, D. Alegre, F. Aumayr, S. Brezinsek, T. Dittmar, K. Dobes, D. Douai, A. Drenik, M. Köppen, U. Kruezi, C. Linsmeier, C. Lungu, G. Meisl, M. Mozetic, C. Porosnicu, V. Rohde, S. Romanelli, Plasma–wall interactions with nitrogen seeding in all-metal fusion devices: Formation of nitrides and ammonia, Fusion Eng. Des. 98–99 (2015) 1371–1374, http://dx.doi.org/10.1016/j.fusengdes.2015.01.044.

[17] R. Simonini, G. Corrigan, G. Radford, J. Spence, A. Taroni, Models and numerics in the multi-fluid 2-D edge plasma code EDGE2D/U, Contrib. Plasma Phys. 34 (2–3) (1994) 368–373, http://dx.doi.org/10.1002/ctpp.2150340242.

[18] D. Reiter, M. Baelmans, P. Börner, The EIRENE and B2-EIRENE codes, Fusion Sci. Technol. 47 (2) (2005) 172–186, http://dx.doi.org/10.13182/FST47-172.

[19] J. Miettunen, M. Groth, T. Kurki-Suonio, H. Bergsåker, J. Likonen, S. Marsen, C. Silva, S. Äkäslompolo, Predictive ASCOT modelling of 10Be transport in JET with the ITER-like wall, J. Nucl. Mater. 438 (2013) S612–S615, http://dx.doi.org/10.1016/j.jnucmat.2013.01.128.

[20] L. Lao, H. St. John, R. Stambaugh, A. Kellman, W. Pfeiffer, Reconstruction of current profile parameters and plasma shapes in tokamaks, Nucl. Fusion 25 (11) (1985) 1611–1622, http://dx.doi.org/10.1088/0029-5515/25/11/007.

[21] N. Horsten, M. Groth, W. Dekeyser, W. Van Uytven, S. Aleiferis, S. Carli, J. Karhunen, K. Lawson, B. Lomanowski, A. Meigs, S. Menmuir, A. Shaw, V. Solokha, B. Thomas, Validation of SOLPS-ITER simulations with kinetic, fluid, and hybrid neutral models for JET-ILW low-confinement mode plasmas, Nucl. Mater. Energy 33 (2022) 101247, http://dx.doi.org/10.1016/j.nme.2022.101247.

[22] R. Mäenpää, H. Kumpulainen, M. Groth, J. Romazanov, B. Lomanowski, S. Brezinsek, S. Di Genova, J. Karhunen, K. Lawson, A.G. Meigs, S. Menmuir, A. Shaw, EDGE2D-EIRENE and ERO2.0 predictions of nitrogen molecular break-up and transport in the divertor of JET low-confinement mode plasmas, Nucl. Mater. Energy 33 (2022) 101273, http://dx.doi.org/10.1016/j.nme.2022.101273.

[23] H.P. Summers, M.G. O'Mullane, Atomic data and modelling for fusion: The ADAS project, AIP Conf. Proc. 1344 (1) (2011) 179–187, http://dx.doi.org/10.1063/1.3585817.

[24] W. Eckstein, D. Heifetz, Data sets for hydrogen reflection and their use in neutral transport calculations, J. Nucl. Mater. 145–147 (1987) 332–338, http://dx.doi.org/10.1016/0022-3115(87)90355-2.

[25] M. Groth, S. Brezinsek, P. Belo, M. Brix, G. Calabro, A. Chankin, M. Clever, J. Coenen, G. Corrigan, P. Drewelow, C. Guillemaut, D. Harting, A. Huber, S. Jachmich, A. Järvinen, U. Kruezi, K. Lawson, M. Lehnen, C. Maggi, C. Marchetto, S. Marsen, F. Maviglia, A. Meigs, D. Moulton, C. Silva, M. Stamp, S. Wiesen, Divertor plasma conditions and neutral dynamics in horizontal and vertical divertor configurations in JET-ILW low confinement mode plasmas, J. Nucl. Mater. 463 (2015) 471–476, http://dx.doi.org/10.1016/j.jnucmat.2014.12.030.

[26] J. Miettunen, M.I. Airila, T. Makkonen, M. Groth, V. Lindholm, C. Björkas, A. Hakola, H.W. Müller, the ASDEX Upgrade Team, Dissociation of methane and nitrogen molecules and global transport of tracer impurities in an ASDEX upgrade L-mode plasma, Plasma Phys. Control. Fusion 56 (9) (2014) 095029, http://dx.doi.org/10.1088/0741-3335/56/9/095029.

[27] D. Reiter, The Data File AMJUEL: Additional Atomic and Molecular Data for EIRENE, vol. 52425, Forschungszentrum Juelich GmbH, 2000.

[28] B.L. Carnahan, W.-W. Kao, E.C. Zipf, A study of the metastable and long-lived Rydberg fragments resulting from electron impact on NH3, J. Chem. Phys. 74 (9) (1981) 5149–5161, http://dx.doi.org/10.1063/1.441724.

[29] R. Snoeckx, J. Tennyson, M.S. Cha, Theoretical cross sections for electron collisions relevant for ammonia discharges part 1: NH_3 , NH_2 , and NH, Plasma Sources Sci. Technol. 32 (11) (2023) 115020, http://dx.doi.org/10.1088/1361-6595/ad0d07.

[30] J. Likonen, M. Airila, E. Alves, N. Barradas, S. Brezinsek, J.P. Coad, S. Devaux, M. Groth, S. Grünhagen, A. Hakola, S. Jachmich, S. Koivuranta, T. Makkonen, M. Rubel, J. Strachan, M. Stamp, A. Widdowson, Jet- Efda Contributors, Deposition of^{13} C tracer in the JET MkII-HD divertor, Phys. Scr. T145 (2011) 014004, http://dx.doi.org/10.1088/0031-8949/2011/T145/014004.

[31] T. Body, S. Cousens, J. Kirby, C. Corr, A volume-averaged model of nitrogen–hydrogen plasma chemistry to investigate ammonia production in a plasma-surface-interaction device, Plasma Phys. Control. Fusion 60 (7) (2018) 075011, http://dx.doi.org/10.1088/1361-6587/aab740.

[32] A. Drenik, L. Laguardia, R. McDermott, G. Meisl, R. Neu, M. Oberkofler, E. Pawelec, R. Pitts, S. Potzel, T. Pütterich, T. Reichbauer, V. Rohde, M. Seibt, G. De Temmerman, R. Zaplotnik, the ASDEX-Upgrade team, the EUROfusion MST1 team, Evolution of nitrogen concentration and ammonia production in N_2 -seeded H-mode discharges at ASDEX upgrade, Nucl. Fusion 59 (4) (2019) 046010, http://dx.doi.org/10.1088/1741-4326/aafe23.

[33] M. Ben Yaala, D.-F. Scherrer, A. Saeedi, L. Moser, K. Soni, R. Steiner, G. De Temmerman, M. Oberkofler, L. Marot, E. Meyer, Plasma-activated catalytic formation of ammonia from N_2 –H_2 : Influence of temperature and noble gas addition, Nucl. Fusion 60 (1) (2020) 016026, http://dx.doi.org/10.1088/1741-4326/ab519c.